

Çukurova Üniversitesi Mühendislik Fakültesi Dergisi

Çukurova University

Journal of the Faculty of Engineering



ISSN: 2757-9255

CILT/VOLUME: 40 SAYI/ISSUE: 2

HAZÍRAN/JUNE 2025

Experimental Investigation of Propeller Effect on Aerodynamic Performance of a Non-slender Delta Wing

Ahmet Ertuğrul BAY 1,a, Tolgay KARA 2,b

¹Gaziantep University, Natural and Applied Sciences, Electrical and Electronics Engineering, Gaziantep, Türkiye

²Gaziantep University, Faculty of Engineering, Department of Electrical & Electronics Engineering, Gaziantep, Türkiye

^aORCID: 0000-0002-5740-7165; ^bORCID: 0000-0003-3991-8524

Article Info

Received: 15.05.2025 Accepted: 26.06.2025

DOI: 10.21605/cukurovaumfd.1699155

Corresponding Author

Ahmet Ertuğrul BAY bay@oprocs.com

Keywords

Propeller effect

Non-slender delta wing

Aerodynamic performance

Static-stability

How to cite: BAY, A.E., KARA, T., (2025). Experimental Investigation of Propeller Effect on Aerodynamic Performance of a Non-slender Delta Wing. Cukurova University, Journal of the Faculty of Engineering, 40(2), 445-452.

ABSTRACT

Propulsion systems are one of the most important components of aircraft that affect their performance. In this research, the effects of propeller effects on aerodynamic forces, aerodynamic performance and moment coefficients of a delta wing with NACA 0012 geometry and sweep angle of 50 degrees in tractor and pusher configurations were investigated and compared with no propeller (base) configuration. The tractor configuration provided the highest lift (0.75 at 4m/s, 0.78 at 6m/s, and 0.85 at 8m/s). The sharp stall phenomenon is not observed in the pusher configuration. The aerodynamic performance (L/D) of the tractor configuration (3.1 at 4m/s, 3.5 at 6m/s and 2.98 at 8m/s) is higher than the pusher configuration (2.18 at 4m/s, 2.66 at 6m/s, and 2.39 at 8m/s) at 12 degrees where they have the maximum L/D ratio. In the pusher configuration, which reattach the separated flow to the surface, the static stability has slightly increased (~0.06 at 8m / s), while in the tractor configuration abrupt changes (~0.2 at 8m/s) are observed depending on the angle of the stall, which requires more attention to the controller design in the UAV design.

İnce Olmayan Delta Kanadın Aerodinamik Performansına Pervane Etkisinin Deneysel Olarak İncelenmesi

Makale Bilgileri

Geliş : 15.05.2025 Kabul : 26.06.2025

DOI: 10.21605/cukurovaumfd.1699155

Sorumlu Yazar

Ahmet Ertuğrul BAY bay@oprocs.com

Anahtar Kelimeler

Pervane etkisi

Nonslender delta kanat

Aerodinamik performans

Statik-karar lılık

Atıf şekli: BAY, A.E., KARA, T., (2025). İnce Olmayan Delta Kanadın Aerodinamik Performansına Pervane Etkisinin Deneysel Olarak İncelenmesi. Çukurova Üniversitesi, Mühendislik Fakültesi Dergisi, 40(2), 445-452.

ÖZ

İtki sistemleri, hava taşıtlarının performansını etkileyen en önemli bileşenlerden biridir. Bu çalışmada, NACA 0012 geometrili ve 50 derece süpürme açısına sahip bir delta kanadın çekici ve itici konfigürasyonlarında pervane etkilerinin aerodinamik kuvvetler, aerodinamik performans ve moment katsayıları üzerindeki etkileri incelenmiş ve pervanesiz (baz) konfigürasyon ile karşılaştırılmıştır. Çekici konfigürasyonu en yüksek kaldırma kuvvetini sağlamıştır (4m/s'de 0,75, 6m/s'de 0,78 ve 8m/s'de 0,85). Maksimum L/D oranına sahip oldukları derecede çekici konfigürasyonunun aerodinamik 12 performansının (L/D) (4m/s'de 3,1, 6m/s'de 3,5 ve 8m/s'de 2,98) itici konfigürasyonundan (4m/s'de 2,18, 6m/s'de 2,66 ve 8m/s'de 2,39) daha yüksek olduğu görülmektedir. Ayrılan akışı yüzeye tekrar bağlayan itici konfigürasyonunda statik kararlılık kararsızlığı biraz (8m/s'de ~0.06) artırırken, çekici konfigürasyonunda stall açısına bağlı olarak ani değişimler (8m/s'de ~0.2) görülmekte, bu da İHA tasarımında kontrolör tasarımına daha fazla dikkat edilmesini gerektirmektedir.

1. INTRODUCTION

In recent years, unmanned aerial vehicles (UAVs) have revolutionized human life with their effective use in military activities such as reconnaissance [1,2], border security [3], search and rescue [4] civilian activities such as logistics [5], advertising [6], agricultural [7], entertainment [8]. This success can be attributed to the design geometries that affect their aerodynamic performance, flight stability and, naturally, the design and efficiency of their propulsion systems. Depending on the environment and mission in which they are to be used, they can be designed as fixed-wing, rotary-wing, unmanned helicopters, flapping-wing, and blimps. One of the most important factors that affect the performance of all these unmanned aircraft systems, regardless of their geometry, is the design of their propulsion systems. Propulsion systems can be analysed under three main headings according to energy type. These are fuel, hybrid, and electric propulsion systems. Electric motors are widely used due to the high power they can produce according to their size, and this use will become even more widespread [9]. Electric motors with ion [10] and plasma [11] thrusters and direct current motors, of which there are many types, are electric motors that generate thrust for aircraft. These electric motors, ion and plasma thrusters, have very low thrust and are used in space applications rather than on earth. [12]. In DC electric motors, they produce thrust using brushless DC motors (BLDC) or permanent magnetic synchronous motors (PMSM). Propeller engine propulsion systems are one of the types of propulsion systems that use these types of motor. Propeller systems are used in a wider range of aircraft, but still at relatively high speeds. For this reason, it is important to investigate the effects of propellers, which are frequently used in propulsion systems in unmanned aerial vehicles, in aircraft design. Propellers create thrust by pushing the air in front of them backward. While multirotor systems rise with this thrust, fixed-wing aircraft travel with this thrust and rise with the air interacting with the wing. The rotational movement of the propeller changes the structure of the air around them. The flows that occur before or after the flow to the propellers are called adapted flows. The flow is adapted before reaching the propeller and the adapted flow passes through the propeller. The propeller positioned at the front of the aircraft is called a tractor, while the propeller positioned at the rear of the aircraft is called a pusher. While the tractor propeller is working under the effect of the wind that has just reached it and adapted from the laminar flow, the pusher propeller adapts the wind flow that has now entered turbulence or is leaving and pushes it through the propeller. Consequently, these interactions have been examined by researchers in the literature. Vries et al. [13] investigated the effects of aerodynamic interactions between propellers on performance and noise in distributed propulsion systems positioned behind the aircraft in a low-turbulence wind tunnel, showing a decrease in efficiency and an increase in noise at close range. Shams et al. 2020 [14] investigated the effect of propeller size on flow and conducted experimental studies with three different propellers with diameters of 5, 6, and 7 inches on a flying-wing designed with a sweep angle of 40 degrees. With this study, they showed that the ratio of propeller diameter to span length, D/b, for values of 22% and higher, the flow dynamics created by the propeller effect and thus contributed significantly to the 6-DoF equation they developed. In a study based on the position of the propeller on the aircraft, Ananda et al. [15] conducted an experiment on square plates with $Re = 6 \times 10^4 - 9 \times 10^4$ different aspect ratio (AR) values and different propellers, and observed a decrease in CL in the tractor configuration of propellers traveling at a speed close to the tunnel speed, while a negligible decrease was observed in the pusher configuration. In their experiments with various propeller and AR configurations, they determined the best lift ratio and optimum AR value and reported that the configuration with these values is the pusher configuration. In another study, Ananda and Selig [16] studied the wing geometry of Wortmann FX-63-137 in tractor and pusher configuration in the range of $Re = 5 \times 10^4 - 3 \times 10^5$. In this study, in the tractor position, the propeller accelerates the air and causes slipstream and as a result, the region behind the propeller enters turbulence faster. In the region not affected by the propeller flow, the separation bubble forms earlier due to this interaction. In this experiment, the researchers reported that at low Reynolds numbers, the tractor configuration obtained much better results than the pusher configuration, L/D and C_L increased, while C_D decreased. Catalano [17] conducted various experiments on the wing model with Wortmann FX-63-137 wing geometry in tractor and pusher configurations. Tractor configuration, angle of attack (AoA) between -4° and 20°, 3.5×10⁵ Reynolds number, 0.28 m chord length, 3 different blade numbers (2, 3 and 4) propellers were used with the same position of the model propellers. In the pusher configuration, experiments were conducted in 7 different positions with a chord length of 0.34 m and a Reynolds number of 4.5×10⁵. In this study, when the pusher configuration was positioned above the propeller chord line and close to the trailing edge, the pusher increased the suction on the propeller blade, prolonged the laminar

flow and reduced the drag resistance. However, the tractor propeller brought forward the transition from laminar to turbulent and increased the turbulence intensity in the boundary layer. In this study, the researcher stated that the pusher configuration is more advantageous. Although Ananda [16] and Catalano [17] proposed different results for the same wing, their studies differ at different Reynolds numbers and in terms of the analysis they target. Ananda [16] based the choice of propeller position on the *L/D* ratio, while Catalano [17] based on the effect of propeller position on flow quality. Chinwicharnam and Thipyopas [18] conducted experiments on NACA 0012 blade with AR=1 at different angles of tilt rotor-fuselage interactions. The effect of propeller on vortices in tractor and pusher configurations at speeds of 20 m/s and 25 m/s in a sharp-edged plate delta wing model with 55° sweep angle have been investigated. In their research, they have observed that the pusher propeller improved the leading-edge vortex better than the tractor propeller and that the propeller advance ratio (J) had an effect on maximum suction. Also, they have observed that C_L increase was higher in the tractor configuration than in the pusher configuration. It is concluded from these studies that the effect of the tractor and pusher configuration on the aerodynamic forces on the wing is directly related to the wing geometry, propeller length, propeller spacing and the propeller effect should be included in micro aerial vehicles (MAVs).

Delta wings are divided into slender and non-slender according to their sweep angles. Delta wings with a sweep angle less than 55° are called non-slender, while wings with a sweep angle greater than 65° are called slender[19]. Non-slender delta wings are highly maneuverable delta wings with sufficient equipment surface and also capable of climbing at high angles [20]. In this study, aerodynamic forces and coefficients of a NACA based non-slender delta wing are investigated under various propeller position such as tractor, and pusher. The thrust generated by motor-propeller is varied from 4 m/s to 8m/s with an increment of 2 m/s. These velocity variations of the motor-propeller on longitudinal stability of the NACA based non-slender delta wing is argued.

2. EXPERIMENTAL SETUP

The model geometry used in the experiment is NACA 0012 non-slender delta wing with 50° sweep angle. Chord of the model is 140 mm and span of the model is 235 mm. The model is produced by using a 3D Printer with 0.2mm nozzle tip. After the production process, the model has been prepared for the experiments by sanding, waxing, and painting processes. Figure 1 shows the model and equipment that are used in the system.

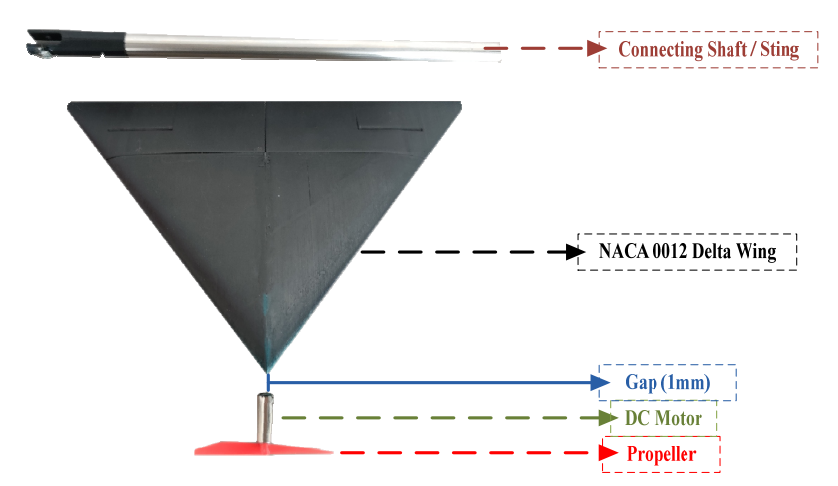


Figure 1. Model and equipment system

The propeller used in the experiment has a length of 74.7 mm and is a two-blade model. In order to study the effect of this propeller on the flow through a certain part of the model, the propeller speed must be equalized with the wind tunnel speed. In order to achieve this equalization, the measurement system shown in Figure 2 was used. In this measurement system, the wind speed generated by the propeller is measured with a pitot tube and these speed values are synchronized with the wind tunnel speed and used in the wind tunnel.

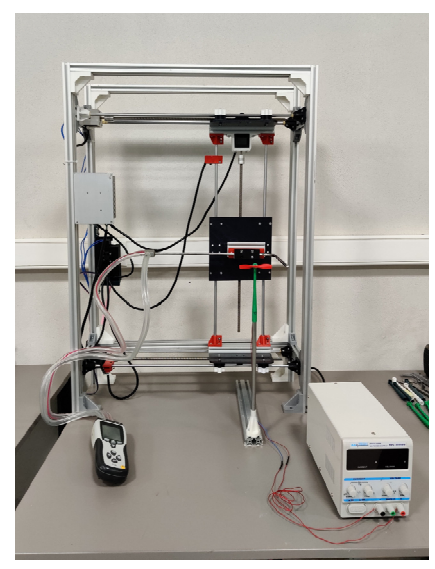


Figure 2. Propeller wind speed measurement system

The experiments were performed in the open-suction wind tunnel shown in Figure 3. The test area where the experiments of the model were carried out measures 40 cm × 40 cm × 100 cm and the experimental setup inside the test area is also shown in Figure 3. The center of gravity of the model was determined and this center of gravity was placed on the 6-axis loadcell with the support of a shaft to determine the aerodynamic forces. Uncertainty analysis of the force calculation experiment is 4.08% and by the calculation for literature [21], and the blockage ratio of the model in the wind tunnel is calculated as 5.14% at the maximum angle of attack in the experiments.



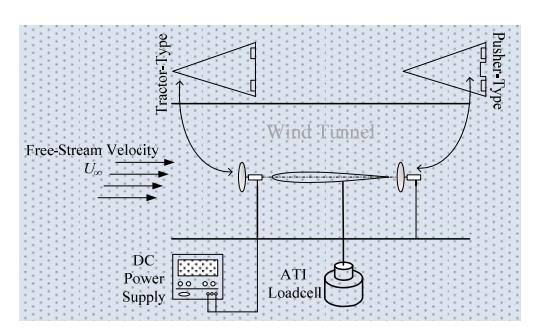


Figure 3. Wind tunnel and model setup with propeller in test section

3. RESULTS AND DISCUSSIONS

In this section, the effect of the propeller placed on the front and rear parts of a symmetric delta wing on the aerodynamic performance was investigated. In addition to the aerodynamic forces, the effects of the propeller on the moment measurements of the model were observed. The lift coefficient is a dimensionless number and it is a ratio of the force acting on the model to the dynamic pressure (q) and planform area (S). The equation of C_L as following Equation 1:

$$C_L = \frac{L}{qS} \tag{1}$$

where, L is the force which is measured by loadcell, $q = \frac{1}{2} \rho V^2$ and S is the planform area of the model. The drag coefficient is the force coefficient acting on the model in the flow direction. The drag coefficient equation is given in Equation 2.

$$C_D = \frac{D}{aS} \tag{2}$$

Measurements were carried out by equalizing the wind tunnel speed to the propeller speed, simulating the flight conditions of the unmanned aerial vehicle. In Figure 4, the situations with the propeller in the front (tractor), in the back (pusher) and without the propeller (base) were measured and compared. In experiments conducted at 4m/s, the stall angle of the base wing model was found to be 18°. The maximum value of the lift coefficient was found to be 0.7518 at 15 degrees in the tractor configuration, 0.6649 at 30 degrees in the pusher configuration, and 0.6196 at 18 degrees in the base model. After the stall angle, the C_L tractor configuration did not experience a dramatic decrease compared to the base model. A stall angle could not be determined for the pusher configuration. Although the drag force coefficients were close to each other up to 12 degrees, after 12 degrees the drag coefficient on the wing started to be less for the pusher configuration. At the stall angle of the base model, the drag of the pusher configuration and the base model were almost equal to each other, while the lowest drag coefficient was observed in the base model after 18°. Analyzing the graphs of 6m/s and 8m/s speed values, it was observed that the stall angle shifted by 3 degrees in tractor and base model configurations. At 6 degrees, C_{Lmax} values were 0.7852 and 0.7031 for tractor and base model, respectively. In the pusher configuration, C_{Lmax} value was found to be 0.7444 at 30 degrees. These values are C_{Lmax} values for the 8 m/s speed measurements and are found to be 0.8502 and 0.7281 respectively. This value increased to 0.7827 in the pusher configuration.

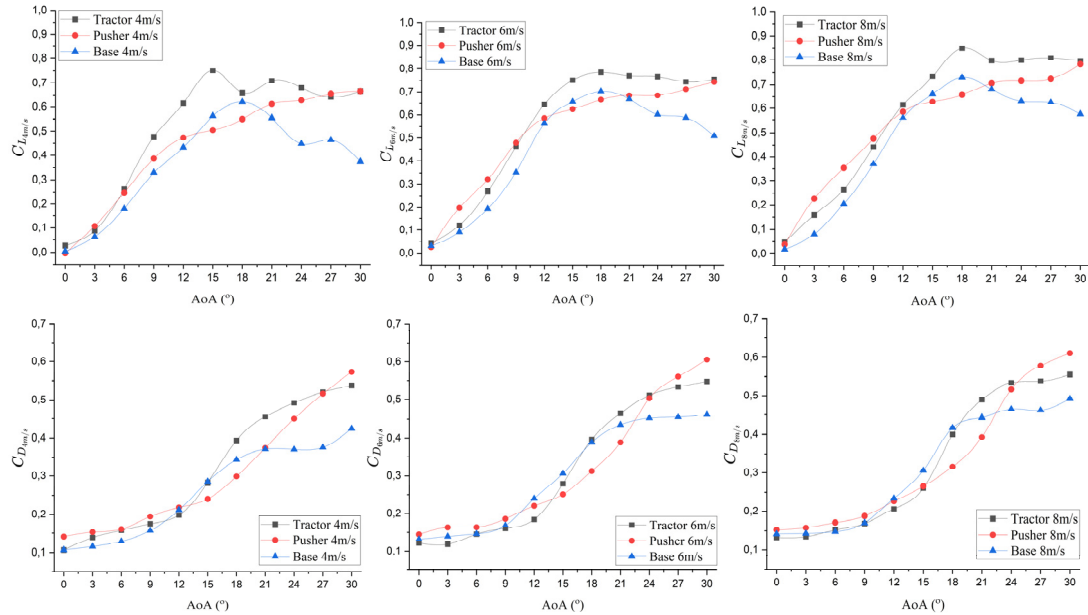


Figure 4. Comparison the effect of propeller position in different freestream velocities

When analyzed according to the drag coefficients, there is a slightly increasing drag coefficient values for all configurations in the 0 - 12 degrees angle of attack range. In the range where the base wing and tractor configurations approach the pre-stall and stall angle values (12-21), the drag coefficient of the pusher configuration is the lowest. Lift and drag coefficients of base model trend is similar to the studies in the literature [22,23].

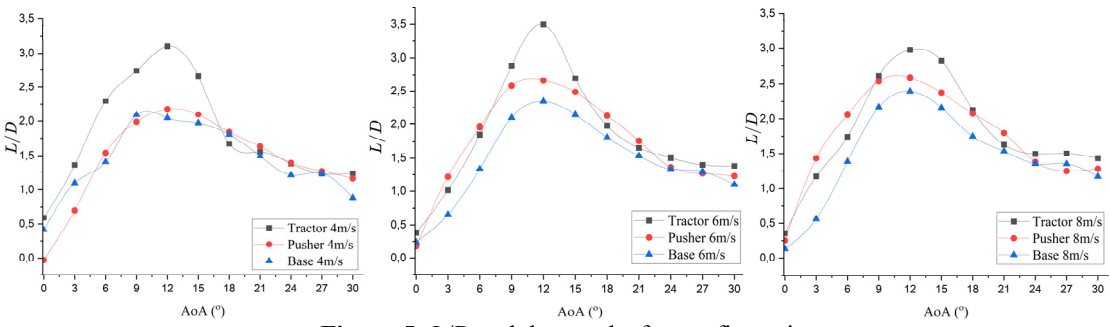


Figure 5. L/D – alpha graphs for configuration

Figure 5 shows the aerodynamic performance (L/D) of the Delta wing at 4m/s, 6m/s and 8m/s. According to these values, the aerodynamic performance of the tractor configuration is the highest. The base model has the maximum L/D ratio at 9 degrees only at 4m/s, while the tractor and pusher configurations have the highest L/D ratios at 12 degrees at 4m/s, 6m/s and 8m/s. When L/D ratios are considered, the tractor configuration has the best ratio. The pusher configuration, in which the turbulent or separated flow in the center of the wing is corrected by the effect of the propeller, is preferred due to the absence of stall angle, which supports the references in the literature [16,17].

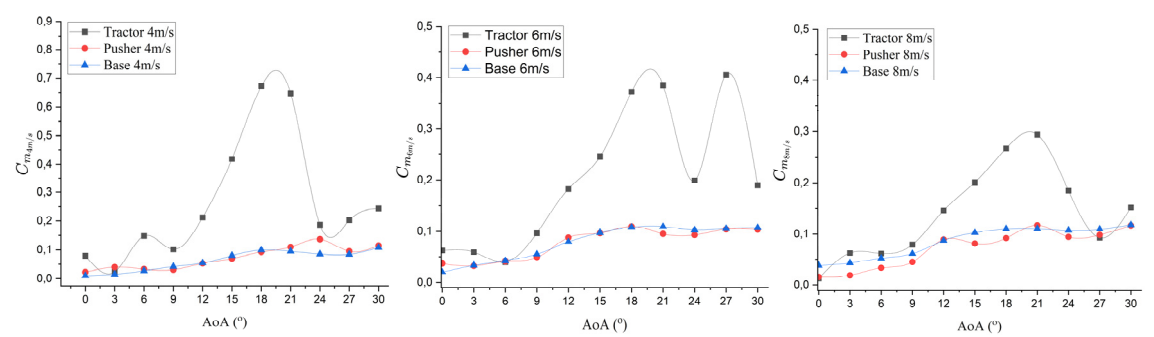


Figure 6. Cm – alpha graph of various configurations of propeller

The moment coefficient is a coefficient of moment that reveals the longitudinal stability of a model or aircraft. The moment coefficient is also called as pitching moment. While it is related to dynamic pressure and planform area like C_L and C_D , the moment coefficient is also related to chord length and is given by Equation 3.

$$C_m = \frac{T_y}{aSc} \tag{3}$$

Where T_y is the moment value obtained by the using loadcell. Figure 6 shows the moment coefficients of the wing at different positions according to the propeller configuration. The base model without propeller has a light neutral moment in the range 0-9 degrees. After 9 degrees, the tip of the delta wing has a downward moment, which increases to 0.1 under the influence of vortices. In the tractor configuration, since the propeller collects the air arriving at the apex of the aircraft and then circulates it turbulently over the wing, it causes high values and sudden changes in the moment coefficient. The fact that at high angle of attacks vortices already start to form at the tip of the nose [24], and that these flows are already unable to adhere to the surface, on top of the disturbing effect of the tractor configuration, explains the moment instabilities. In the pusher configuration, the moment coefficients are relatively stable due to the effect of the propeller to attach the flow separated from the surface to the surface. Considering the C_m analysis of the pusher configuration for the longitudinal static stability analysis, it is seen that the effects of the reduction of the drag force between 12-18 degrees are in the direction of static stability in the Cm-alpha graph.

4. CONCLUSION

A NACA 0012 non-slender delta wing with a 50° sweep angle and a chord length of 140 mm was manufactured and experiments were performed at wind tunnel speeds of 4m/s, 6m/s and 8m/s. In order to investigate the effects of propeller flow on aerodynamic forces, experiments were conducted with the wind tunnel speed to equalize the propeller speed. In these experiments, the propeller was placed in tractor and pusher configurations and measurements were performed. As a result of these experiments, the findings for the NACA 0012 delta wing are as follows.

- When the aerodynamic performance, lift and drag coefficients of the base model are compared with the propeller configurations, it is observed that there are significant differences in values such as C_{Lmax} , L/D_{max} . It is evident from the differences that it is a must to investigate the propeller effects especially when designing MAVs.
- The tractor configuration has a higher lift coefficient than the pusher configuration. At 8m/s, the lift coefficient is 0.8502 at 18 degrees for the tractor configuration. It is 0.6568 in pusher configuration at

- the same angle value. In the pusher configuration, the maximum lift coefficient increases to 0.7827 at 30 degrees, but since the drag force increases with this increase, the L/D ratio decreases.
- In terms of aerodynamic performance comparison, the configuration with the highest *L/D* ratio was the tractor configuration. It is 2.98 at tractor configuration and 2.59 in pusher configuration at 8m/s experiments.
- It appears that sharp stall phenomenon is not observed in pusher configuration. Thus, it can be said that it can be used as a reason for preference in missions where high aerodynamic performance is not required.
- In this statically-unstable model, the static stability of the base model and pusher configuration has a smooth graph in the direction of instability, while the tractor configuration has sudden moment changes.

5. REFERENCES

- 1. Iscold, P., Pereira, G.A.S. & Torres, L.A.B. (2010). Development of a hand-launched small UAV for ground reconnaissance. *IEEE Transactions on Aerospace and Electronic Systems*, 46(1), 335-348.
- **2.** Murat, M. ve Öztürk, F. (2024). Kısa pistli uçak gemilerinden operasyonel olarak IHA kaldırmak için maliyet etkin bir yaklaşım. *Çukurova Üniversitesi Mühendislik Fakültesi Dergisi*, *39*(1), 23-30.
- **3.** Koslowski, R. & Schulzke, M. (2018). Drones along borders: border security UAVs in the united states and the european union. *International Studies Perspectives*, 19(4), 305-324.
- **4.** Silvagni, M., Tonoli, A., Zenerino, E. & Chiaberge, M. (2017). Multipurpose UAV for search and rescue operations in mountain avalanche events. *Geomatics, Natural Hazards and Risk*, 8(1), 18-33.
- **5.** Li, Y., Liu, M. & Jiang, D. (2022). Application of unmanned aerial vehicles in logistics: a literature review. *Sustainability*, 14(21), 14473.
- **6.** Ullah, F., Al-Turjman, F., Qayyum, S., Inam, H. & Imran, M. (2021). Advertising through UAVs: optimized path system for delivering smart real-estate advertisement materials. *International Journal of Intelligent Systems*, 36(7), 3429-3463.
- 7. Tsouros, D.C., Bibi, S. & Sarigiannidis, P.G. (2019). A review on UAV-based applications for precision agriculture. *Information*, 10(11), 349.
- **8.** Kim, S.J., Jeong, Y., Park, S., Ryu, K. & Oh, G. (2018). A survey of drone use for entertainment and AVR (augmented and virtual reality), in augmented reality and virtual reality. *Springer International Publishing, Cham*, 339-352.
- **9.** Zhang, B., Song, Z., Zhao, F. & Liu, C. (2022). Overview of propulsion systems for unmanned aerial vehicles. *Energies*, *15*(2), 455.
- **10.** Polk, J., Anderson, J., Brophy, J., Rawlin, V., Patterson, M., Sovey, J. & Hamley, J. (1999). An overview of the results from an 8200 hour wear test of the nstar ion thruster. *35th Joint Propulsion Conference and Exhibit*.
- 11. Charles, C. (2009). Plasmas for spacecraft propulsion. *Journal of Physics D: Applied Physics*, 42(16), 163001.
- 12. Levchenko, I., Goebel, D., Pedrini, D., Albertoni, R., Baranov, O., Kronhaus, I., Lev, D., Walker, M.L.R., Xu, S. & Bazaka, K. (2025). Recent innovations to advance space electric propulsion technologies. *Progress in Aerospace Sciences*, 152, 100900.
- **13.** De Vries, R., Van Arnhem, N., Sinnige, T., Vos, R. & Veldhuis, L.L.M. (2021). Aerodynamic interaction between propellers of a distributed-propulsion system in forward flight. *Aerospace Science and Technology*, *118*, 107009.
- **14.** Shams, T.A., Shah, S.I.A., Shahzad, A., Javed, A. & Mehmod, K. (2020). Experimental investigation of propeller induced flow on flying wing micro aerial vehicle for improved 6dof modeling. *IEEE Access*, 8, 179626-179647.
- **15.** Ananda Krishnan, G.K., Deters, R.W. & Selig, M.S. (2014). Propeller-induced flow effects on wings of varying aspect ratio at low reynolds numbers. *32nd AIAA Applied Aerodynamics Conference*.
- **16.** Ananda, G.K., Selig, M.S. & Deters, R.W. (2018). Experiments of propeller-induced flow effects on a low-reynolds-number wing. *AIAA Journal*, *56*(8), 3279-3294.
- 17. Catalano, F.M. (2004). On the effects of an installed propeller slipstream on wing aerodynamic characteristics. *Acta Polytechnica*, 44(3). 8-14.
- **18.** Chinwicharnam, K. & Thipyopas, C. (2016). Comparison of wing–propeller interaction in tractor and pusher configuration. *International Journal of Micro Air Vehicles*, 8(1), 3-20.
- **19.** Gursul, I. (2005). Review of unsteady vortex flows over slender delta wings. *Journal of Aircraft*, 42(2), 299-319.

- **20.** Tümse, S. & Bilgili, M. (2021). Lift coefficient estimation of a delta wing under the ground effect using artificial neural network. *Çukurova Üniversitesi Mühendislik Fakültesi Dergisi*, 36(3), 625-636.
- **21.** Coleman, H.W. (2018). Experimentation, validation, and uncertainty analysis for engineers. *John Wiley & Sons, Incorporated*, Newark.
- **22.** Tumse, S., Tasci, M.O., Karasu, I. & Sahin, B. (2021). Effect of ground on flow characteristics and aerodynamic performance of a non-slender delta wing. *Aerospace Science and Technology*, 110, 106475.
- 23. Taylor, G.S. & Gursul, I. (2004). Buffeting flows over a low-sweep delta wing. AIAA Journal, 42(9), 1737-1745.
- **24.** Gursul, I., Gordnier, R. & Visbal, M. (2005). Unsteady aerodynamics of nonslender delta wings. *Progress in Aerospace Sciences*, 41(7), 515-557.